Robotica (2014) volume 32, E2, pp. 1–24. © Cambridge University Press 2014
doi:10.1017/S0263574714002501

Motion planning for a rapid mobile manipulator using model-based ZMP stabilization

Dongil Choi and Jun-ho Oh

†*The Robotics Institute, Carnegie Mellon University, Pittsburgh, PA, USA*
‡*HUBO Laboratory (Humanoid Robot Research Center), Korea Advanced Institute of Science and Technology (KAIST), Daejeon, South Korea*

(Accepted September 24, 2014)

SUMMARY
This paper introduces a novel approach to motion planning for a rapid mobile manipulator using inverted pendulum models. Our aim was to realize an actual rapid mobile manipulator with high acceleration and speed performance for an object's delivery. In our research, we developed an actual rapid mobile manipulator called KDMR-1. We proposed simple motion planning methods using a single inverted pendulum model (SIPM) and a double inverted pendulum model (DIPM), which are easily adaptable to a real-time system with only a small computational burden. The SIPM was useful for basic movement but did not provide object carrying capability. For that, a DIPM was proposed. In both models, we designed linear quadratic optimal controllers to stabilize the Zero Moment Point (ZMP). Two kinds of ZMP stabilization strategies were proposed, fixed ZMP and relaxed ZMP. Using these strategies, we realized optimal ZMP stabilizations for a real-time rapid mobile manipulator. For decoupled forward and rotational linear DIPM, we designed a centrifugal acceleration compensation model in the manner of feedback linearization. The experimental results showed high acceleration and speed performances during rapid object delivery.

KEYWORDS: Wheeled robots; Service robots; Manipulation planning.

1. Introduction

Currently, many mobile robots use a statically stable four-wheel drive system. Mobile robots usually have high CoM (Center of Mass) in order to interact with humans, and such mobile robots have a high rate of rollover during rapid acceleration. To prevent rollover, mobile robots typically are designed with a low CoM and a wide ground-contact area. This kind of mobile robot has a pyramidal shape for a low profile, and is a common design among service robots. Despite these design efforts, mobile robots exhibit quite a low level of performance in terms of acceleration capabilities.

The stabilization of mobile robots has been a topic of particular interest, and for stable and rapid movement, it is necessary to develop a dynamic stabilization algorithm. Stabilization methods for a stationary vehicle were studied using the conventional optimal time trajectory planning of a manipulator,[1,2] and the stabilization methods of a moving redundant manipulator were proposed using the ZMP criterion.[3,4] In other studies, degrees for stability measures were proposed.[5,6] Some research efforts have focused on high speed (over 12 km/hr) and acceleration (over 0.5 g, 1 g = 9.8m/s^2) performance; however, it has been difficult to implement a roll-over algorithm in a real-time system due to the complexity of the algorithm or the lack of an actual rapid mobile manipulator.[3,4,7,8]

In our previous research,[9–11] we proposed the ZMP stabilization method of a rapid four-wheel mobile platform for high acceleration performance using an inverted pendulum model. We achieved a maximum acceleration of 0.5 g and maximum velocity of 12 km/hr despite the high CoM. The motion planning method using an inverted pendulum model is simple, but widely used. Kajita[12] designed a walking pattern using the inverted pendulum model with a preview controller to stabilize ZMP. His walking pattern algorithm was adapted to HRP-2. Sugihara[13] used the inverted pendulum

* Corresponding authors. E-mails: doyle.choi.cdi@gmail.com, jhoh@kaist.ac.kr

Table I. The system properties depending on the models and strategies.

	Fixed ZMP	Relaxed ZMP
SIPM	1. No torque applied on the pendulum for zero ZMP change	1. Large torque applied on the pendulum for flexible motion maintaining ZMP inside supporting polygon
	2. High acceleration but Bad maneuverability due to reverse action	2. Good maneuverability with low acceleration
	3. Max 0.8 g and 13.0 km/hr	3. Max 0.25 g and 2.9 km/hr
	4. No object carrying capability	4. No object carrying capability
DIPM	1. Small torque on pendulum 1 to remove double reverse action, no torque on pendulum 2 for zero ZMP change	1. Large torque on pendulum 1 to flexible motion maintaining ZMP inside supporting polygon, no torque on pendulum 2 for zero ZMP change
	2. High acceleration but Bad maneuverability due to reverse action	2. Good maneuverability with low acceleration
	3. Max 0.56 g and 13 km/hr	3. Max 0.2 g and 2.9 km/hr
	4. Stable object carrying	4. Stable object carrying

model to generate a real-time walking pattern. Park[14] designed a real-time walking pattern using the ZMP equation of the simple inverted pendulum model, and this walking pattern was implemented on KHR-3 (HUBO). The strength of the motion planning method using the inverted pendulum model is simple enough to apply to a real-time system, and also guarantees ZMP stability.

In this paper, we addressed the motion planning of a rapid mobile manipulator for object delivery using simple inverted pendulum models. We have developed an actual rapid mobile manipulator called KDMR-1. The development of KDMR-1 is addressed in appendix A1. Simple inverted pendulum models were proposed to control the rapid mobile manipulator in real-time. In the single inverted pendulum model (SIPM), we used decoupled linear models, with the assumption that the forward and rotational movements are controlled independently. The SIPM provided limited stabilization for an object on the end-effector. The SIPM was useful for basic movement but did not provide object carrying capability. To stabilize the object on the end-effector, we used a double inverted pendulum model (DIPM). The DIPM produced better results for keeping the end-effector stable. In both models, we designed controllers to stabilize the ZMP of a rapid mobile manipulator using two different strategies, a *fixed* ZMP strategy and a *relaxed* ZMP strategy. Using these strategies, we realized optimal ZMP stabilizations of a real-time rapid mobile manipulator. The fixed ZMP strategy produces some reverse motion due to the non-minimum phase property of system, whereas the relaxed ZMP strategy does not produce the behavior. The fixed ZMP strategy involves a large penalty on the torque applied to the pendulum so that very little torque is applied to the pendulum. As a result, very little ZMP change is guaranteed so that the higher acceleration is possible. On the contrary, the relaxed ZMP strategy involves a small penalty on the torque, therefore the torque applies on the pendulum somehow and there is ZMP change, but it provide better tracking on the reference input without reverse motion. In the Table I, the system properties depending on the models and strategies are summarized.

To stabilize the coupled movement of the forward and rotational movement, we designed a centrifugal acceleration compensation model. Through a feedback linearization of the centrifugal acceleration, we guaranteed that the rapid mobile manipulator can be stabilized by decoupled forward and rotational linear DIPMs with stable object delivery. Experiments were conducted to evaluate the proposed methods.

2. Model Description

2.1. SIPM (single inverted pendulum model)

2.1.1. Description of SIPM. In Fig. 1, the 5-DOF manipulator is simplified as a SIPM (Single Inverted Pendulum Model) with mass m_p. The mobile platform with two caster wheels is simplified as m_c. There are two reference frames: one is a Newtonian reference frame, N, and the other is a local frame,

https://doi.org/10.1017/S0263574714002501 Published online by Cambridge University Press

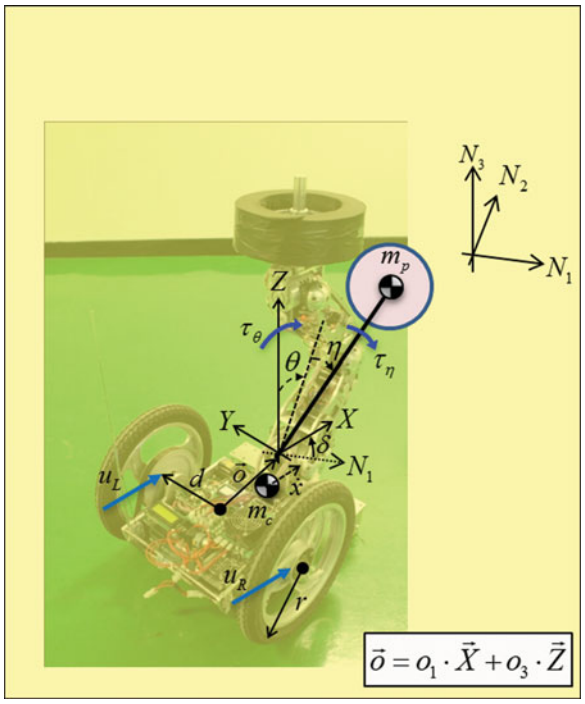

Fig. 1. (Colour online) Free body diagram of the rapid mobile manipulator.

XYZ, located on the origin of the manipulator. The mobile platform moves in the X direction and rotates on the Z axis. The X direction position is defined as x, and the rotation of the mobile platform on the Z axis (Yaw direction) is defined as δ. The rotation on the Z axis of the mobile platform causes lateral movement along the Y axis, the local frame on the origin of the manipulator, due to the offset from the origin of the axis, o_1. The inverted pendulum can rotate on the X axis (roll direction) and the Y axis (pitch direction). The rotation angle on the pitch direction is defined as θ, and the rotation angle on the roll direction is defined as η. The torque input on the pitch direction is τ_θ, and the torque input on the roll direction is τ_η. The force input for the left wheel is u_L, and for the right wheel is u_R. The control inputs on both wheels are produced by motors inside the mobile platform. The rotational torque of the mobile platform is produced by driving the control inputs on both wheels differentially. The vector $\vec{o}$ indicates the offset from the center of the rotation of the mobile platform to the origin of the manipulator.

The SIPM has 4-DOF, and its configuration is given by the variables x, δ, θ, η. We derived the equation of motion using 'Autolev' software.[15] In this case, the equation of motion is quite complex and highly coupled. For the first attempt, we made two assumptions to simply the problem:

ASSUMPTIONS: (For SIPM)

1) The inclined angle of the inverted pendulum θ, η is small enough to linearize.

→ This assumption is usually valid for a rotation angle under 30°. If the angle is 30° (0.5236rad), sin(30°) is 0.5rad. Therefore, we can assume sin(30°) $\cong \theta$ under 30°. Therefore, we restricted the moving range of the inverted pendulum to less than 30°.

2) We did not account for a coupled motion of the mobile manipulator in the SIPM. It means that the forward movement along X direction and the rotational movement on the Z axis does not happen at the same time.

→ The coupled motion is quite complex to solve; therefore, we considered decoupled motions. The X axis forward movement and the Z axis rotational movement were dealt with using an independent linearized equation of motions on the local frame. For this, we assumed that the rotation angle, δ, can be linearized at $\delta = 0$.

From assumptions 1 and 2, the rotation angle of the inverted pendulum model on the pitch and roll direction was linearized at $\theta = 0, \eta = 0$ and the rotational angle of the mobile platform was

https://doi.org/10.1017/S0263574714002501 Published online by Cambridge University Press

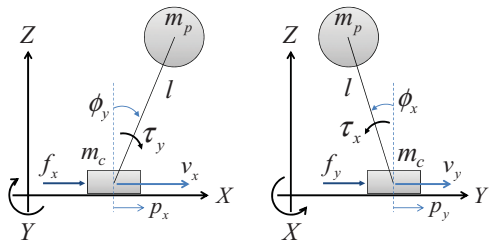

Fig. 2. (Colour online) The SIPM of pitch joints and roll joints, respectively.

linearized at $\delta = 0$. From the assumptions above, the linearized equations of motion of the rapid mobile manipulator were derived as follows:

$$\left(m_c + m_p\right)\ddot{x} + m_p l \cdot \ddot{\theta} = u_L + u_R \quad \left(I_2 + m_p l^2\right)\ddot{\theta} + m_p l \cdot \ddot{x} - m_p g l \cdot \theta = \tau_\theta \tag{1}$$

$$\left(I_3 + J_3 + m_p o_1^2\right)\ddot{\delta} - m_p o_1 l \cdot \ddot{\eta} = d\left(u_R - u_L\right) \quad \left(I_1 + m_p l^2\right)\ddot{\eta} - m_p o_1 l \cdot \ddot{\delta} - m_p g l \cdot \eta = \tau_\eta \tag{2}$$

Equation (1) is a linearized equation referring to the forward movement along the X axis, and Eq. (2) is a linearized equation referring to the rotational movement on the Z axis of the mobile manipulator. The lateral velocity along the Y axis $\dot{y}$ is generated by the rotational velocity of the mobile platform on the Z axis $\dot{\delta}$ when the mobile platform rotates on the spot. Therefore, we can construct the following equation:

$$\dot{y} = o_1 \cdot \dot{\delta} \tag{3}$$

From relationship (3), we can reorganize Eq. (2) as follows:

$$\left(\frac{I_3 + J_3}{o_1^2} + m_p\right)\ddot{y} - m_p l \cdot \ddot{\eta} = \frac{d}{o_1}\left(u_R - u_L\right) \quad \left(I_1 + m_p l^2\right)\ddot{\eta} - m_p l \cdot \ddot{y} - m_p g l \cdot \eta = \tau_\eta \tag{4}$$

We can determine that Eq. (4) is exactly the same as Eq. (1). The differences between linearized equation of pitch joints and linearized equation of roll joints are due to the direction of rotation of the inverted pendulum. Equation (4) is basically a linear model for the lateral movement along the Y axis. The rotational movement on the Z axis is converted to the lateral movement along the Y axis on the local frame. We will call the rotational movement on the Z axis as the lateral movement along the Y axis in the rest of the paper. The Eq. (1) can be considered as the SIPM of pitch direction projected on the XZ plane and Eq. (4) can be considered as the SIPM of roll direction projected on the YZ plane. The decoupled models projected on pitch and roll direction are presented in Fig. 2. The forward velocity of the cart along the X axis is redefined as v_x and the pitch angle of the inverted pendulum is redefined as ϕ_y. The lateral velocity of the cart along the Y axis is redefined as v_y and the roll angle of the inverted pendulum is redefined as ϕ_x. The force input to the mobile platform along the X axis and the Y axis is redefined as f_x, f_y, respectively, and the torque of the inverted pendulum along the Y axis and the X axis is redefined as τ_y, τ_x, respectively.

The state-space equation of the SIPM of the pitch direction becomes as follows:

$$\dot{x}_x = A_x x_x + B_x u_x \quad x_x = \left[\, v_x \quad \phi_y \quad \dot{\phi}_y \,\right]^T, \quad u_x = \left[\, f_x \quad \tau_y \,\right]^T. \tag{5}$$

This is a linear model for forward movement along the X axis. On the other hand, the state-space equation of the SIPM of the roll direction becomes as follows:

$$\dot{x}_y = A_y x_y + B_y u_y \quad x_y = \left[\, v_y \quad \phi_x \quad \dot{\phi}_x \,\right]^T, \quad u_y = \left[\, f_y \quad \tau_x \,\right].^T \tag{6}$$

This is a linear model for lateral movement along the Y axis. The ZMP equations on each model are as follows, respectively:

$$p_x = -\frac{\tau_y}{\left(m_p + m_c\right) g}, \; p_y = \frac{\tau_x}{\left(m_p + m_c\right) g}. \tag{7}$$

https://doi.org/10.1017/S0263574714002501 Published online by Cambridge University Press

We can design basically the same controllers on both models. Our inverted pendulum model is very similar to one of Kajita's models.[12] The main difference between Kajita's model and ours is the existence of the torque input on the inverted pendulum. They only used the jerk of CoM of the inverted pendulum as a control input, in which case the inverted pendulum becomes a free rotating joint. In this case, the ZMP becomes the center of rotation of the inverted pendulum and p_x, p_y always remains zero.

In our research, however, the SIPM has two inputs. One is the force on the mobile platform and the other is the torque on the inverted pendulum. To stabilize an inverted pendulum model and the ZMP of the system, we used a state-feedback controller. The state-feedback gain can be found using the linear quadratic optimal control method. By changing the weighting matrix, we can tune the non-minimum phase characteristic of the inverted pendulum model in two ways: the *fixed ZMP strategy* and the *relaxed ZMP strategy*.

In the assumption of the SIPM, we considered that the forward and lateral movements are controlled independently. Actually, this assumption is only valid when the forward and lateral movements do not occur simultaneously, and when the pure forward movement along the *X* axis and the pure lateral movement along the *Y* axis are possible, as with an Omni-directional drive system. However, in our differential drive system, the nonlinear centripetal accelerations are real when the forward and lateral movements are coupled. If the stable ZMP region is sufficient, the actual system can be stabilized using the SIPM, even though we have over-simplified assumptions. However, for object delivery, the centrifugal accelerations should be compensated effectively. To compensate centrifugal acceleration terms, we considered the feedback linearization method on the (DIPM) in the next section.

2.2. DIPM (double inverted pendulum model)

2.2.1. Problem statement. The rapid mobile manipulator can be used for rapid object delivery in open spaces like conference halls, shopping malls, hospitals and so on. We placed an object on the end-effector to be delivered without bonding. In the previous section, the manipulator were modeled as the SIPM. In this section, we controlled the manipulator using DIPMs (Double Inverted Pendulum Models) to stabilize the ZMP of the end-effector.

If we assume that there is no torque input on the inverted pendulum, we can control the ZMP to coincide to the origin of the inverted pendulum. This is absolutely true because, by definition, ZMP is zero moment point. The ZMP of the no torque inverted pendulum is, by its nature, the origin of the inverted pendulum. By using this natural phenomenon, we can control the dual ZMP of the system simply using the DIPM.

In the case of coupled movement, which is forward and lateral movement occurring simultaneously, the centrifugal accelerations are real. In DIPMs, we can compensate for the centrifugal accelerations with the feedback linearization method.

2.2.2. Feedback linearization for model decoupling. To compensate for the centrifugal acceleration, we made the following assumptions:

ASSUMPTIONS: (For DIPM)

1) The left and right wheels do not slip on the ground.

→ We used the differential drive system for the mobile platform, which has two active wheels on the rear and two caster wheels on the front. We assumed that there was a non-slip condition on the active wheels.

2) The centrifugal accelerations are compensated by a feedback linearization method.

→ Rather than ignoring the coupled movement, we planned centrifugal acceleration compensating algorithms to decouple the combined forward and lateral movement in the manner of feedback linearization.

3) We dealt with decoupled movement by using linear models.

→ Using the feedback linearization method to decouple the coupled movement, we can use simple linear models to control the forward and lateral movement independently.

For a differential drive system, we can consider the above kinematic relationship as shown in Fig. 3. The ICC indicates the Instantaneous Center of Curvature and D is the instantaneous radius of curvature. $\dot{\psi}$ is an angular velocity centered on the ICC with radius D. The velocity on the left wheel,

https://doi.org/10.1017/S0263574714002501 Published online by Cambridge University Press

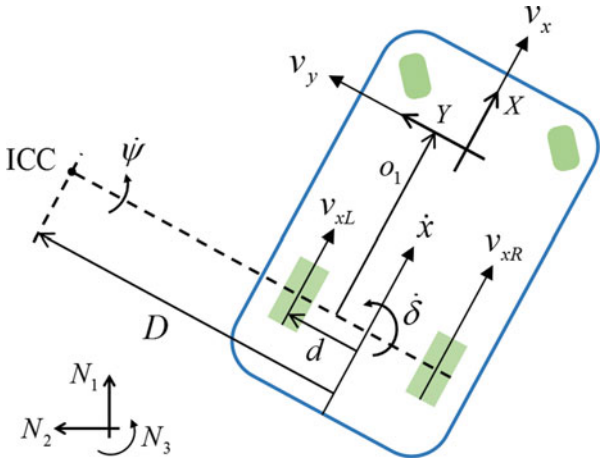

Fig. 3. (Colour online) Kinematic relationship of the differential drive system.

v_{xL}, and the velocity on the right wheel, v_{xR}, are expressed as the following equations under the assumption that both wheels make contact with no slippage.

$$v_{xL} = \dot{x} - d\dot{\delta} \quad v_{xR} = \dot{x} + d\dot{\delta} \tag{8}$$

Also from the ICC, the velocities on both wheels can be expressed in another form, as follows:

$$v_{xL} = (D - d)\dot{\psi} \quad v_{xR} = (D + d)\dot{\psi} \tag{9}$$

From Eqs. (8) and (9), we find the following relationship:

$$\dot{x} = D\dot{\psi} \quad \dot{\psi} = \dot{\delta}. \tag{10}$$

This indicates that the angular velocity at the ICC is identical to the angular velocity at the center of the axle in the differential drive system with nonslip conditions. In this differential drive system, the velocity and acceleration on the origin of the XY frame are expressed as follows:

$$v_x = \frac{v_{xL} + v_{xR}}{2} = D\dot{\psi} = \dot{x} \quad v_y = \dot{y} = o_1\dot{\delta}, \tag{11}$$

$$a_x = \ddot{x} - o_1\dot{\delta}^2 \quad a_y = \ddot{y} + \dot{x}\dot{\delta}. \tag{12}$$

In acceleration Eq. (12), the first terms are linear accelerations along the X, Y axis, respectively, and the second terms are centripetal accelerations. The linear acceleration along the X axis can be regarded as a longitudinal acceleration, while the linear acceleration along the Y axis can be regarded as a lateral acceleration. The centripetal acceleration along the X axis is induced by the offset, o_1. There are no Coriolis terms because there is only one rotating frame, $\dot{\psi} = \dot{\delta}$, under the nonslip conditions.

If the mobile manipulator is moving with the acceleration conditions above, the centrifugal acceleration on the end-effector can be depicted as in Fig. 4.

The centrifugal acceleration is equal to the centripetal acceleration in the opposite direction, as follows:

$$a_{cx} = o_1\dot{\delta}^2 \quad a_{cy} = -\dot{x}\dot{\delta} = -\frac{\dot{x}^2}{D} = -\frac{v_x^2}{D}. \tag{13}$$

In case that the centrifugal acceleration and the gravitational acceleration are applied as depicted in Fig. 4, there are compensating angles, θ_{cy}, θ_{cx}, to make zero moment. The compensating angles

https://doi.org/10.1017/S0263574714002501 Published online by Cambridge University Press

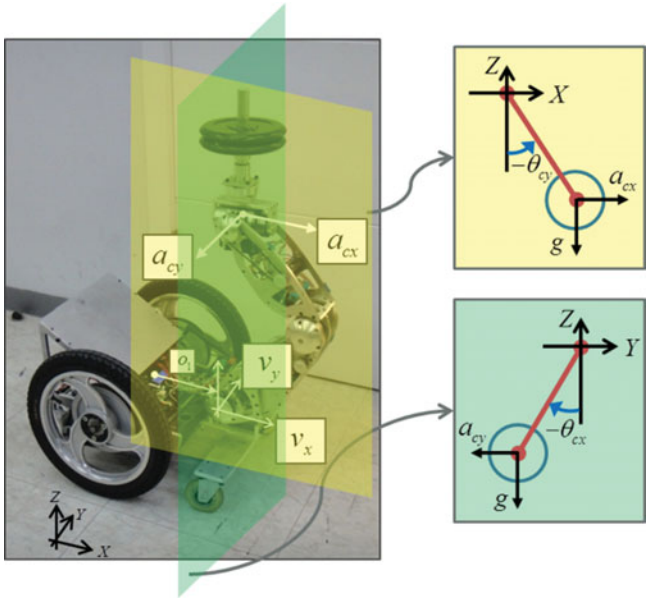

Fig. 4. (Colour online) Centrifugal accelerations on the end-effector.

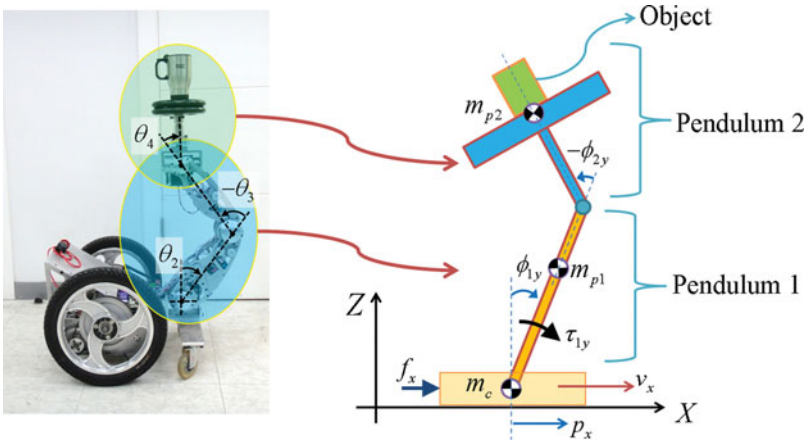

Fig. 5. (Colour online) DIPM for forward movement.

are calculated according to a simple kinematic relationship, as follows:

$$\theta_{cy} = -\tan^{-1}\left(\frac{a_{cx}}{g}\right) \quad \theta_{cx} = -\tan^{-1}\left(\frac{a_{cy}}{g}\right). \tag{14}$$

With these desired angles, the centrifugal acceleration exerted on the end-effector are compensated. As a result, the forward and lateral movement in DIPM can be dealt with decoupled systems. The overall control scheme of DIPM with feedback linearization is addressed in Section 3.2.

2.2.3. Description of DIPM. There are two ZMPs to be controlled. One is the ZMP of the mobile manipulator on the ground and the other is the ZMP of the end-effector that stabilizes the object. By assuming two pitch joints, (θ_2, θ_3), as pendulum 1 and one pitch joint, (θ_4), and the object as pendulum two, we constructed a DIPM for forward movement, as shown in Fig. 5. As we addressed previous section, we decoupled the forward and lateral movement based on the feedback linearization method. The DIPM can be applied to the forward and lateral movement independently. On our first attempt, we dealt with the forward movement of the mobile manipulator.

The DIPM in Fig. 5 has two control inputs. One is the force, f_x, to control the mobile platform and the other is the torque, τ_{1y}, on pendulum 1. There is no torque in pendulum 2. Because the supporting

https://doi.org/10.1017/S0263574714002501 Published online by Cambridge University Press

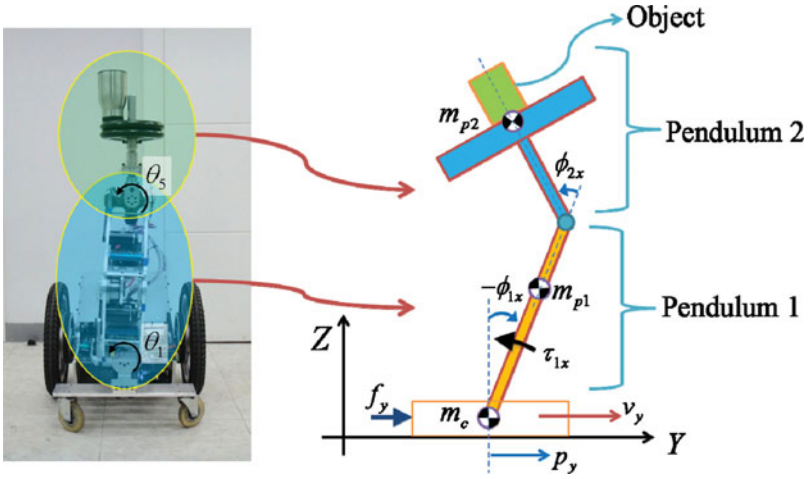

Fig. 6. (Colour online) DIPM for lateral movement.

polygon of the mobile platform is much larger than that of the end-effector, we made pendulum 2 a no torque inverted pendulum. In no torque inverted pendulum, the ZMP is fixed to the origin. On the other hand, in pendulum 1, we can use the torque input on it for the relaxed ZMP strategy.

We used a small angle assumption for linearization. The rotation angle of the double inverted pendulum were under 30°, small enough to linearize. From this assumption, the linearized state-space equation of forward movement is expressed as the following:

$$\begin{aligned} \dot{X}_x &= A_x X_x + B_x U_x \\ X_x &= \begin{bmatrix} v_x & \theta_{1y} & \dot{\theta}_{1y} & \theta_{2y} & \dot{\theta}_{2y} \end{bmatrix}^T, \\ U_x &= \begin{bmatrix} f_x & \tau_{1y} \end{bmatrix}^T \end{aligned} \tag{15}$$

Secondly, DIPM for lateral movement is depicted in Fig. 6. There are two roll joints in our mobile platform. The first roll joint, (θ_1), becomes pendulum 1 and the second joint, (θ_5), and the object become pendulum 2. The force and torque input configuration is the same as the forward movement. The linearized state-space equation of rotational movement can be expressed as:

$$\begin{aligned} \dot{X}_y &= A_y X_y + B_y U_y \\ X_y &= \begin{bmatrix} v_y & \theta_{1x} & \dot{\theta}_{1x} & \theta_{2x} & \dot{\theta}_{2x} \end{bmatrix}^T, \\ U_y &= \begin{bmatrix} f_y & \tau_{1x} \end{bmatrix}^T \end{aligned} \tag{16}$$

We can apply the same control structure to both forward and lateral models independently. In the next section, we designed a fixed or relaxed ZMP strategy for DIPMs using the state feedback controller.

3. Motion Planning for a Rapid Mobile Manipulator

3.1. Motion planning using SIPM

The target system researched in this paper has a four-wheel drive system. It consists of a support polygon in a two-dimensional space through connections of four points on the ground. If the ZMP is located inside the support polygon, the system is stable.[8,16,17] Otherwise, the system is prone to roll.

https://doi.org/10.1017/S0263574714002501 Published online by Cambridge University Press

We redefined the state-space equation of SIPMs to include outputs as the following forms:

$$\begin{aligned}
\dot{x} &= Ax + Bu \\
y &= Cx + Du \\
x &= [\, v \quad \phi \quad \dot{\phi}\,]^T, u = \begin{bmatrix} f & \tau \end{bmatrix}^T \\
y &= \begin{bmatrix} v & p \end{bmatrix}^T
\end{aligned} \tag{17}$$

We ignored the subscription x, y because the linear models for forward and lateral movement have exactly the same structure. The SIPM mentioned above is an MIMO (multi-input multi-output) system, which has two inputs: f, τ, and two outputs: v, p. This system has an unstable pole. To stabilize an inverted pendulum and the ZMP of the system, we designed the LQR (Linear-Quadratic Regulator) controller gain, K, to minimize the quadratic cost function, J.

$$u = K\,(x_d - x) \tag{18}$$

$$J = \int_0^\infty \left(x^T Q x + u^T R u\right) dt, \tag{19}$$

where $x_d = [\, v^{\text{des}}\ 0\ 0\,]^T$. The Q is the weighting matrix for the state and R is the weighting matrix for the control inputs. The associated Riccati equation is:

$$0 = A^T S + SA - SB \cdot R^{-1} \cdot B^T S + Q. \tag{20}$$

By using the solution of the Riccati equation, S, we obtained the optimal feedback gain, K, as:

$$K = R^{-1} B^T S. \tag{21}$$

We simulated the state-feedback controller in Fig. 7 by changing the weighting matrices. At first, we set the weighting matrices of fixed approach as:

$$Q = \begin{bmatrix} 1 & 0 & 0 \\ 0 & 0 & 0 \\ 0 & 0 & 0 \end{bmatrix}, \quad R = \begin{bmatrix} 3 \times 10^{-5} & 0 \\ 0 & 10^2 \end{bmatrix}. \tag{22}$$

The result of velocity tracking simulation of fixed ZMP is expressed on the left side of Fig. 7. In the simulation, we applied a desired velocity, v_x^{des}, as 3.5m/sec (12.6 km/hr) at 1 s. We can see undershoot on the velocity graph. We will refer to this undershoot as a reverse action. Basically, this is a non-minimum phase characteristic of the inverted pendulum due to a right-half plane zero. This type of undershoot is undesirable in a typical system, because it creates a large tracking error in the transient state. To overcome this problem, Kajita[12] used a preview control, and Napoleon[18] used two masses for the inverted pendulum model. In our research, however, we accepted this reverse action, because it has the positive effect of pushing the inverted pendulum forward more quickly by moving the mobile platform backward. We call this type of ZMP control strategy the *fixed ZMP strategy.*

The fixed ZMP strategy causes the system to accelerate more dynamically. We observed a maximum acceleration at about 0.7 g, with a maximum velocity of 3.5m/sec (12.6 km/hr). The ZMP, p_x is normalized from -1 to 1. Here, '0' indicates that the ZMP is located at the center of the support polygon, and '1' or '-1' signifies that the ZMP is located on the edge of the support polygon. In the weighting matrix R, the weighting about the force input is much smaller than that of the torque input. This indicates that a large penalty is applied on the torque input. Eventually, the force input is dominant, and the torque input is almost zero in the fixed approach. As a result, the ZMP coincides with the origin of the inverted pendulum. To maintain the ZMP on the origin of the inverted pendulum, the reverse action is inevitable. As a result, the ZMP is fixed on the initial position in the fixed ZMP strategy.

https://doi.org/10.1017/S0263574714002501 Published online by Cambridge University Press

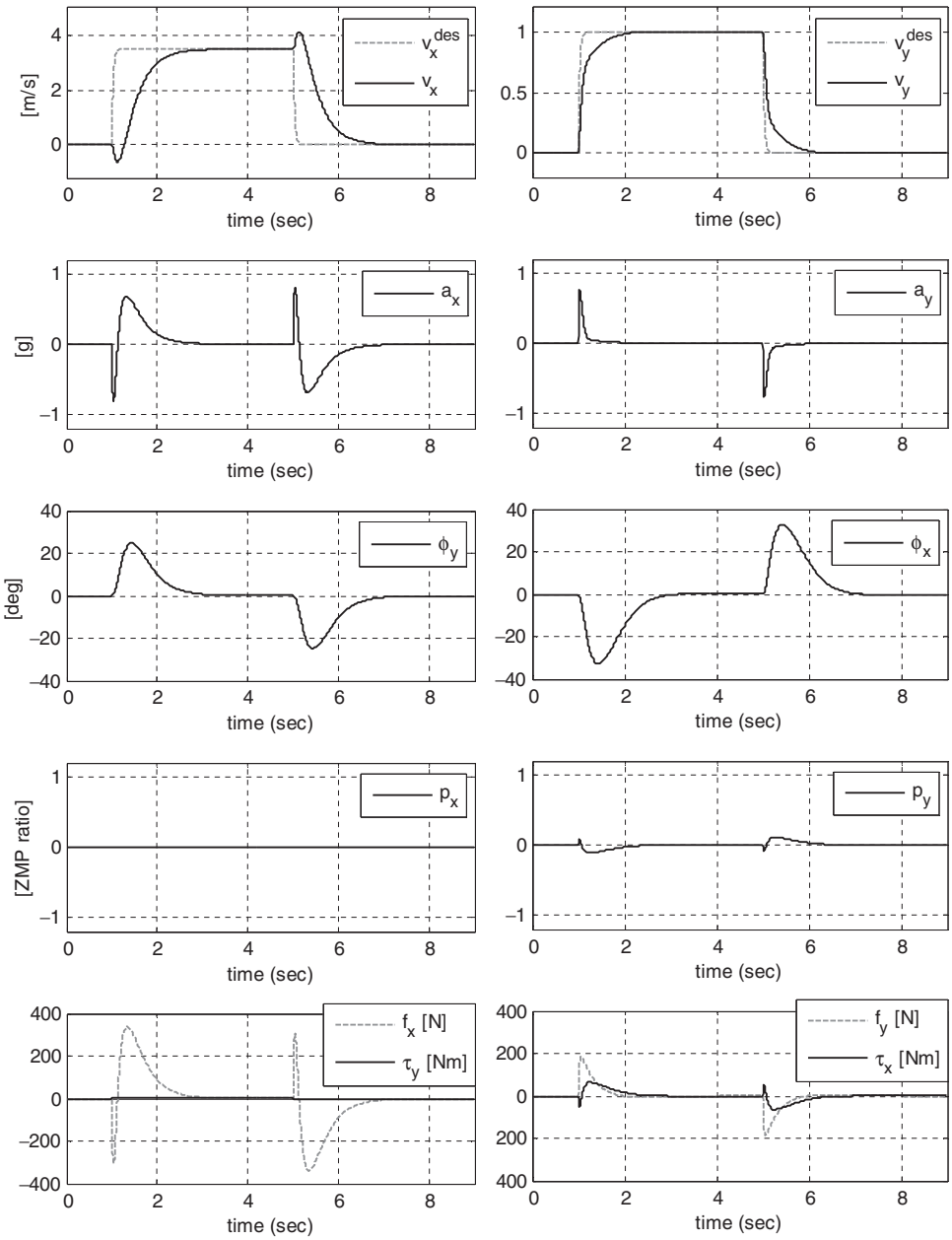

(a) Fixed **(b) Relaxed**

Fig. 7. Linearized simulation results of SIPM depending on weighting matrices. (a) Fixed (b) Relaxed.

Secondly, we set the weighting matrices of the relaxed approach as:

$$Q = \begin{bmatrix} 1 & 0 & 0 \\ 0 & 0 & 0 \\ 0 & 0 & 0 \end{bmatrix}, \quad R = \begin{bmatrix} 10^{-5} & 0 \\ 0 & 10^{-5} \end{bmatrix}. \tag{23}$$

The result of velocity tracking simulation of relaxed ZMP is expressed on the right side of Fig. 7. We applied a desired velocity as 1 m/sec at 1 s. The ZMP does not maintain zero, and the inverted pendulum rotates in the opposite direction compared to its rotation in the fixed approach. The reverse action disappears in the relaxed approach, and the weighting of the force input is the same as that of the torque input in the relaxed approach. As a result, both the force input and the torque input are

https://doi.org/10.1017/S0263574714002501 Published online by Cambridge University Press

Table II. Pros and Cons of the fixed and relaxed ZMP strategies.

	Fixed ZMP strategy	Relaxed ZMP strategy
Pros	1. Zero ZMP change 2. Dynamic acceleration	1. Good maneuverability 2. Flexible motion
Cons	1. Bad maneuverability due to the reverse action	1. Relatively high fluctuation of the ZMP

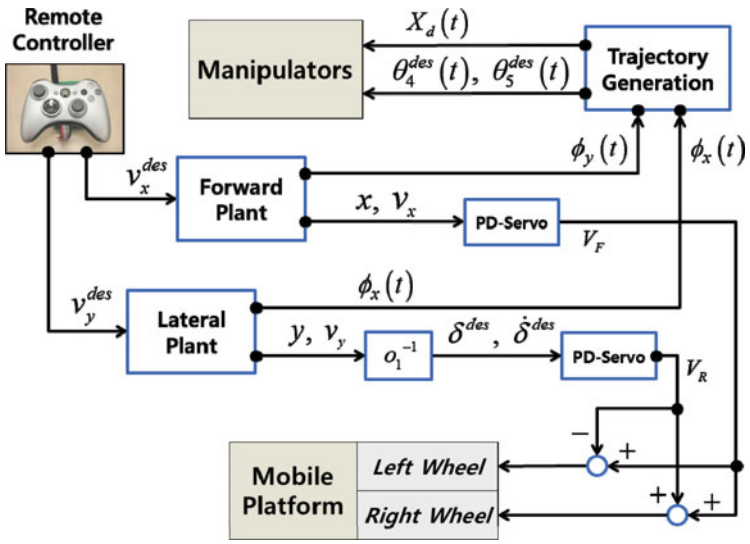

Fig. 8. (Colour online) Overall control scheme of the SIPM.

valid for controlling the inverted pendulum model. Due to the torque input, it can track the desired velocity without the reverse action. The stability of the system is guaranteed, because the ZMP, p_y is located inside the supporting polygon.[8,16,17] In this control strategy, we allow of ZMP change inside the supporting polygon. We will refer to this kind of ZMP stabilizing strategy as the *relaxed ZMP strategy*.

The span from the front to the rear wheels is 0.3m. The span from one left wheel to one right wheel is 0.5m. The fixed approach is suitable for forward movement, because it requires rapid and dynamic acceleration performance and the span is relatively short. The relaxed approach is suitable for lateral movement, because the stable area of the ZMP is large enough to apply the relaxed ZMP strategy, and it provides good maneuverability without reverse action. The pros and cons of the fixed and relaxed ZMP strategies are summarized in Table II.

The overall control scheme using the SIPMs is shown in Fig. 8. In each model, the feed-forward motion trajectories are generated by proposed linear models. The motion trajectory of the manipulator is given as follows:

$$X_d(t) = \left[x_p^{\text{des}}(t) \quad y_p^{\text{des}}(t) \quad z_p^{\text{des}}(t) \right]^T . \tag{24}$$

The desired velocity of forward direction along the X axis, v_x^{des}, and the desired angular velocity for rotation about the Z axis, $\dot{\delta}^{\text{des}}$, is given by a remote controller. The desired velocity of forward direction, v_x^{des}, is applied to the 'Forward Plant'. From the forward plant, the pitch angle of the inverted pendulum, ϕ_y, generated by SIPM and this angle is converted to the motion trajectory using the following equation:

$$x_p^{\text{des}}(t) = L_e \cdot \sin\left\{\phi_y(t)\right\}, \tag{25}$$

where the length from the origin to the end-effector is L_e(0.48m in KDMR-1). The forward movement of the mobile platform is controlled by the PD-servo as the position and velocity of the forward plant, x, v_x.

https://doi.org/10.1017/S0263574714002501 Published online by Cambridge University Press

The desired lateral velocity along the Y axis, v_y^{des}, is applied to the 'Lateral Plant'. The resultant roll angle of the inverted pendulum, ϕ_x, in the lateral plant is converted to the motion trajectory for the roll joints using the following equation:

$$y_p^{\text{des}}(t) = L_e \cdot \sin\{\phi_x(t)\}. \tag{26}$$

The origin of the manipulator is located on the front of the mobile platform. The offset is defined as o_1 in Fig. 1. The desired rotational angle and velocity of the mobile platform about the Z axes, δ^{des}, $\dot{\delta}^{\text{des}}$, is simply calculated by dividing y, v_y into the offset o_1. The rotation of the mobile platform about the Z axis is controlled by the PD-servo. We applied the differential voltage input to the left and right wheels using the following rotational voltage input:

$$V_R = K_p^w \cdot \left\{\delta^{\text{des}} - \delta\right\} + K_v^w \cdot \left\{\dot{\delta}^{\text{des}} - \dot{\delta}\right\}, \tag{27}$$

where K_p^w, K_v^w are the position and velocity gains of the PD-servo, respectively.

The change in height is approximately 64 mm when the inclined angle of the inverted pendulum is 30°, which is the maximum linearization range. Therefore, the change in height can be ignored and the manipulator maintains a constant level. The motion trajectory of the manipulator along the Z axis is as follows:

$$z_p^{\text{des}}(t) = L_e. \tag{28}$$

We controlled the orientation of the end-effector with the following desired segment angle trajectories:

$$\theta_4^{\text{des}}(t) = -\{\theta_2(t) + \theta_3(t)\} + \phi_y(t) \quad \theta_5^{\text{des}}(t) = -\theta_1(t) \tag{29}$$

The first joint angle configuration in Eq. (29) keeps the pitch orientation of the end-effector equal to the rotation angle of the inverted pendulum of the forward plant. The second joint angle configurations in Eq. (29) maintain the roll orientation of the end-effector perpendicular to the ground. For the control of the orientation, we used a PD-servo.

3.2. Motion planning using DIPM

In the previous section, we showed through simulations that the rapid mobile manipulator can accelerate about 0.7 g. At this acceleration, we can stabilize the rapid mobile manipulator using linear SIPMs. In the weighting matrix of the fixed approach of the SIPM, the torque input was almost zero. From this fixed ZMP strategy, we found that the ZMP can be controlled simply to match the origin by the no torque model. However, we could not stabilize the object on the end-effector using these SIPMs. Global stability can be secured by the SIPM, but for object stability, we needed additional stabilization using DIPM.

For DIPM, we used the same linear quadratic optimal control method as in SIPM. At first, we explored the forward movement of DIPM. In the weighting matrix of the fixed approach, we set the weighting matrices as:

$$Q = \begin{bmatrix} 1 & 0_{1\times4} \\ 0_{4\times1} & 0_{4\times4} \end{bmatrix}, \quad R = \begin{bmatrix} 3\times10^{-5} & 0 \\ 0 & 1\times10^{2} \end{bmatrix}. \tag{30}$$

The weighting matrix for control input, R is the same as that of the SIPM using the fixed ZMP strategy. The result of the velocity tracking simulation of fixed ZMP is expressed on the left side of Fig. 9. The desired velocity is given at 1 s as 3.5m/sec. On the velocity graph, we can observe double changing of the direction at 1 s. This is the reverse action due to the non-minimum phase characteristic of the double inverted pendulum. In this simulation, the torque input for pendulum 1 is almost zero. Therefore, the DIPM becomes a purely no torque double inverted pendulum. As a result, the reverse action occurs twice. We call this *double reverse action*. It is more difficult to control the velocity of the mobile platform in the double reverse action than in the single reverse action.

https://doi.org/10.1017/S0263574714002501 Published online by Cambridge University Press

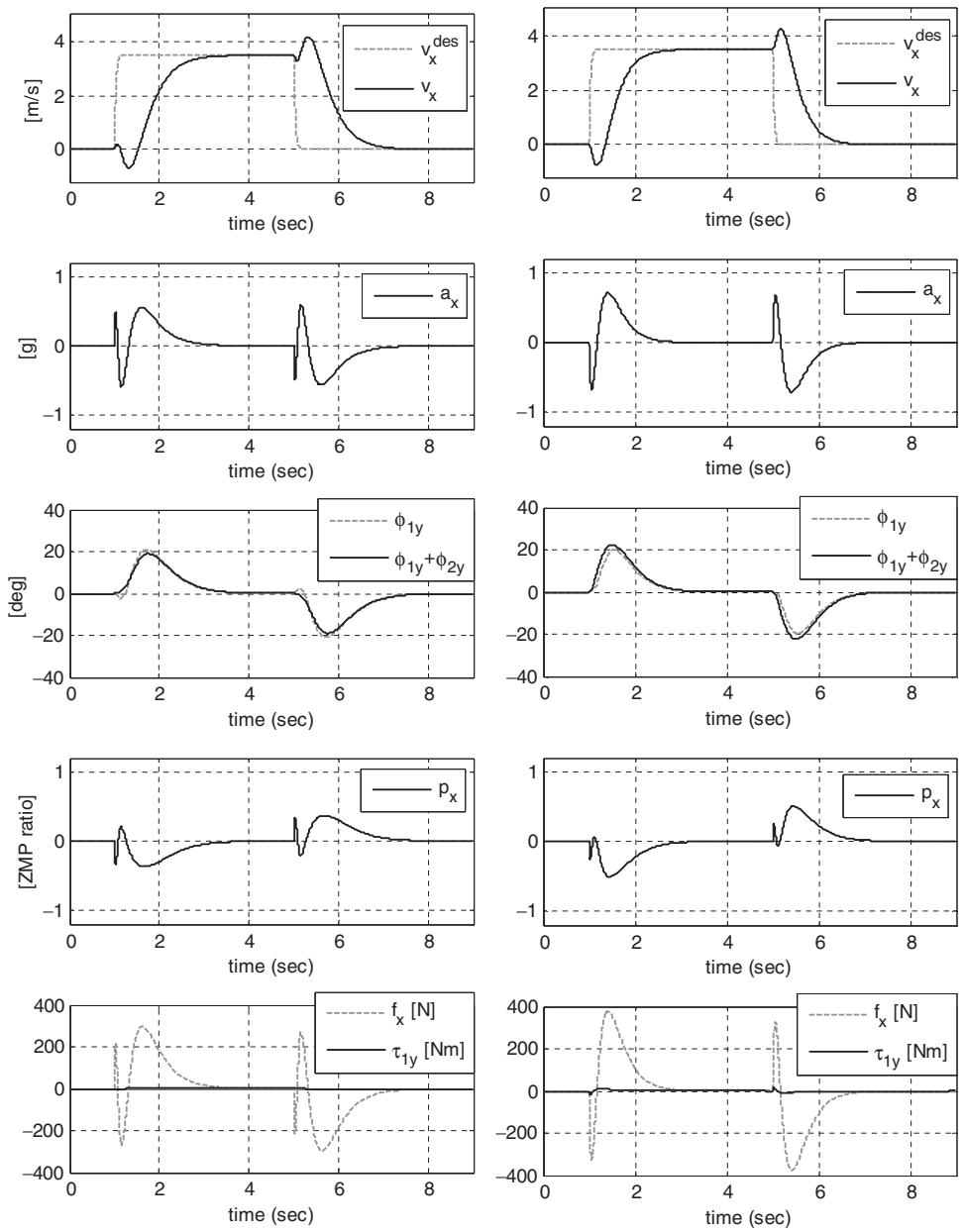

(a) Fixed-1 **(b) Fixed-2**

Fig. 9. Linearized simulation results of DIPM of forward movement. (a) Fixed-1 (b) Fixed-2.

To avoid the double reverse action, we redefine the weighting matrices, as follows:

$$Q = \begin{bmatrix} 1 & 0_{1\times 4} \\ 0_{4\times 1} & 0_{4\times 4} \end{bmatrix}, \quad R = \begin{bmatrix} 1\times 10^{-5} & 0 \\ 0 & 1\times 10^{-2} \end{bmatrix}. \tag{31}$$

In this configuration, the weighting for torque input in R matrix is smaller than that of Eq. (30). As a result, the penalty on torque input has decreased. The result of the velocity tracking in these weighting matrices is shown on the right side of Fig. 9. In this result, the double reverse action has disappeared. Instead, the reverse action is similar to SIPM. The torque input of pendulum 1 is very small value. However, it can eliminate the double reverse action. The maneuverability was enhanced and the ZMP, p_x was controlled within the stable region. The segment angle of pendulum 2 is similar to the angle of pendulum 1, but it is not exactly the same. The ZMP of pendulum 2 is always located on

https://doi.org/10.1017/S0263574714002501 Published online by Cambridge University Press

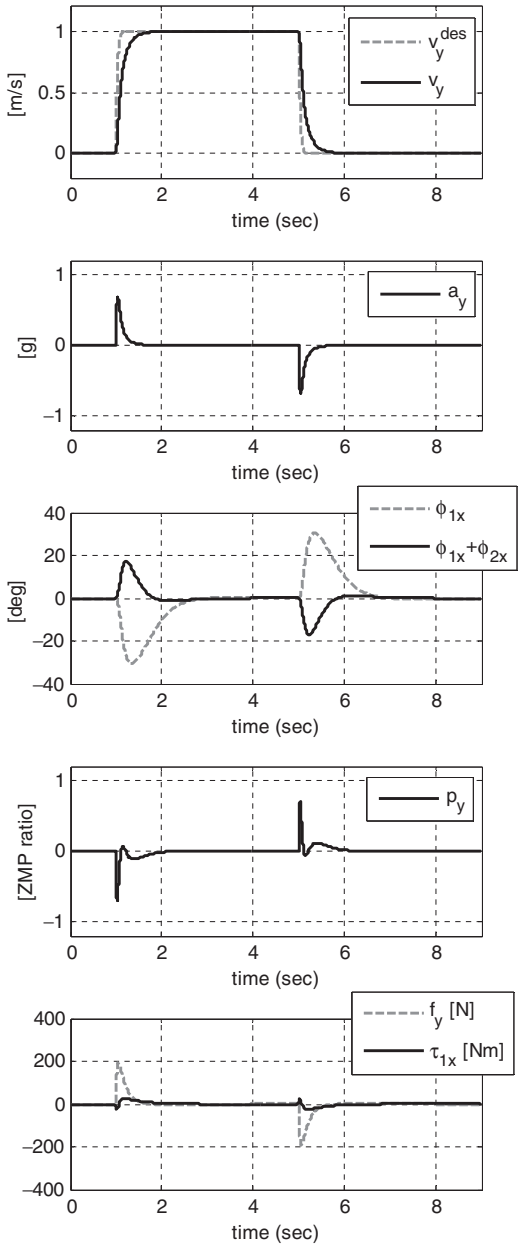

Fig. 10. Linearized simulation result of DIPM of lateral movement.

the origin of pendulum 2, because pendulum 2 does not have torque input. Using this control strategy, we stabilized the forward movement of the mobile platform and the object on the end-effector at the same time and achieved a maximum acceleration of 0.7 g and maximum velocity of 12.6 km/hr.

Secondly, let us consider the lateral movement. In this weighting matrix of the relaxed approach, we set the weighting matrices as:

$$Q = \begin{bmatrix} 1 & 0_{1\times 4} \\ 0_{4\times 1} & 0_{4\times 4} \end{bmatrix}, R = \begin{bmatrix} 1\times 10^{-5} & 0 \\ 0 & 1\times 10^{-5} \end{bmatrix}. \tag{32}$$

The weighting matrix for control input, R is the same as that of the SIPM using the relaxed ZMP strategy. The result of the velocity tracking simulation is shown in Fig. 10.

The desired velocity, v_y^{des}, is given at 1 s as 1m/sec. The velocity tracked the desired trajectory without reverse action, and the inclined angle of pendulum 1 showed a typical relaxed ZMP strategy.

https://doi.org/10.1017/S0263574714002501 Published online by Cambridge University Press

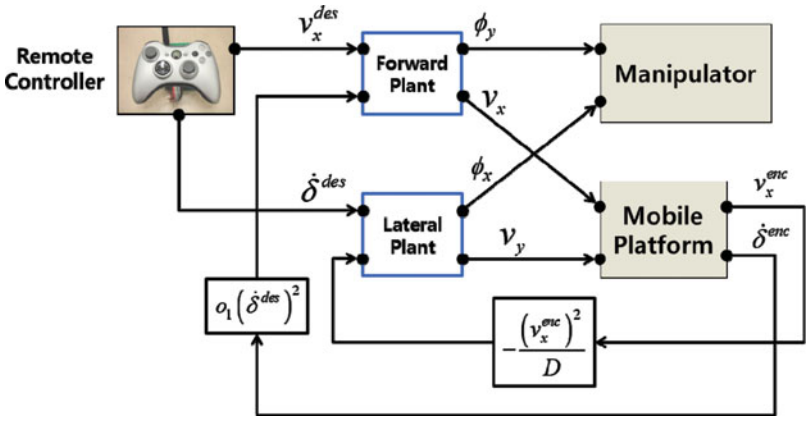

Fig. 11. (Colour online) Overall control scheme of the DIPM.

Using the torque input, τ_{1x}, pendulum 1 was controlled flexibly and the ZMP, p_y remained within the stable region. In the case of pendulum 2, the ZMP maintains the origin all the time because of no torque condition. As a result, we stabilized the lateral movement and the object on the end-effector in the manner of the relaxed ZMP strategy.

The motion trajectory for the manipulator was given the same way as in the SIPM. Using the angle of pendulum 1, the desired trajectory of the manipulator along the *X*, *Y* axis was generated. The height of the manipulator maintained a constant level. The orientation of the end-effector was controlled as follows:

$$\theta_4^{\text{des}}(t) = -\{\theta_2(t) + \theta_3(t)\} + \{\phi_{1y}(t) + \phi_{2y}(t)\} + \theta_{cy}$$
$$\theta_5^{\text{des}}(t) = -\theta_1(t) + \{\phi_{1x}(t) + \phi_{2x}(t)\} + \theta_{cx} \tag{33}$$

Each desired angle is defined as a segment angle. The centrifugal acceleration compensating angles, θ_{cy}, θ_{cx}, were superimposed with the orientation angles from DIPMs.

The overall control scheme using the DIPMs is shown in Fig. 11. 'Forward Plant' refers to the DIPM for the forward movement along the *X* axis and 'Lateral Plant' refers to the DIPM for the lateral movement along the *Y* axis. From the remote controller, the desired forward velocity, v_x^{des}, and the desired rotational velocity, $\dot{\delta}^{\text{des}}$, is applied to DIPMs. From two DIPMs, feed-forward trajectories for the mobile platform and the manipulator are generated independently. From the mobile platform, the actual rotational velocity, $\dot{\delta}^{enc}$ and the actual forward velocity, v_x^{enc} are measured by encoders on the left and right wheels. The measured rotational and forward velocities are fed back to forward and lateral plants to compensate for the centrifugal accelerations. From this feedback linearization method, the coupled movement can be controlled using decoupled forward and lateral DIPMs.

Rapid object delivery experiments using DIPMs were conducted to prove the effectiveness of the proposed methods.

4. Experiments

4.1. Rapid movement using SIPM

4.1.1. Forward movement using SIPM. We carried out a rapid maneuvering experiment using KDMR-1. We used the fixed ZMP strategy of SIPM proposed in Section 3.1 for forward movement. The actual behavior of KDMR-1 in this experiment is available in the webpage. (https://sites.google.com/site/dongilc27/research).

Initially, the 5-DOF manipulator has a basic bent posture. During acceleration, the inverted pendulum moves forward with the reverse action of the mobile platform. At a constant speed, it maintains the basic posture. The inverted pendulum moves backward as it stops. After it stops, the manipulator reverts to its basic posture.

https://doi.org/10.1017/S0263574714002501 Published online by Cambridge University Press

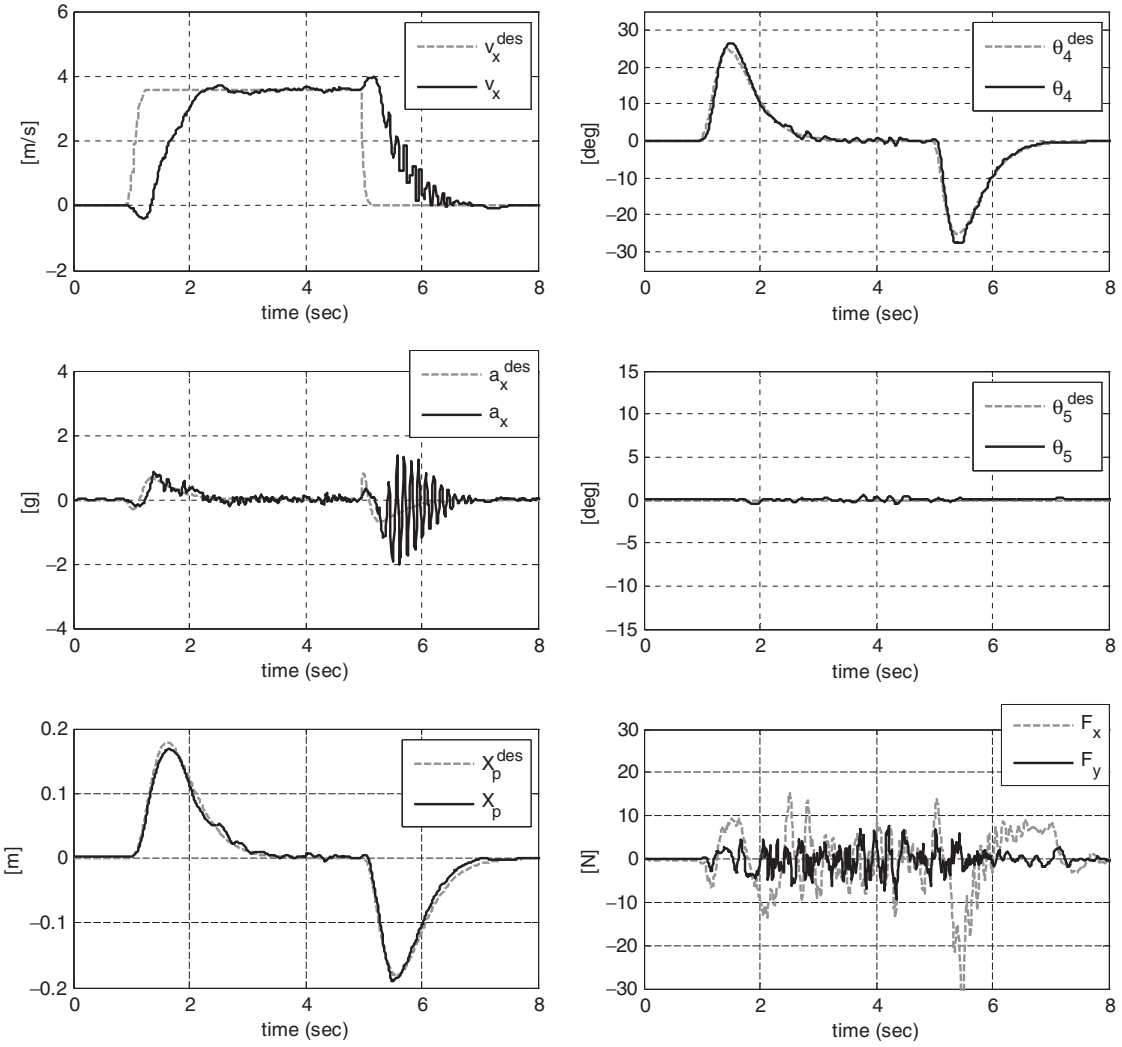

Fig. 12. Graphical results of forward movement experiment using the SIPM.

Figure 12 shows graphs of the forward movement. The dashed line is a model value and the solid line is an actual value from the mobile platform. The manipulator was controlled by the Cartesian computed torque control. The Cartesian computed torque method gains were determined experimentally to have under-damped characteristics for suspension-like motion[11,19,22] as follows: $K_p = 200$, $K_v = 20$ on the X axis; $K_p = 30$, $K_v = 8$ on the Y axis; and $K_p = 30$, $K_v = 7$ on the Z axis. The desired forward velocity was applied at 1 s as 3.6 m/s (about 13 km/hr) and the desired rotational velocity was fixed as zero. We can observe that the actual velocity was well controlled by the desired value with the reverse action. The position of the end-effector along the X axis tracked the desired value quite precisely due to the comparably high gain on the Cartesian computed torque control. The vibration during the deceleration period was due to slippage between the ground and tires. We obtained a maximum forward velocity of 13 km/hr and maximum forward acceleration of 0.8 g, ignoring the vibration during the deceleration period. The segment angle of the end-effector, θ_4, θ_5, is controlled according to Eq. (29). We confirmed that the orientation angle was well controlled at the desired value.

Using the FT sensor developed in our previous research,[19] we measured the disturbance moments on the end-effector accounting the moment arm (0.21 m in KDMR-1) and those moments are converted to the disturbance forces, F_x, F_y. From this force information, we can evaluate the ZMP stability indirectly. The disturbance force is actually a moment along the Y, X axis. Therefore, if the disturbance forces are small, we can trust that the end-effector is controlled stably in terms of ZMP.

https://doi.org/10.1017/S0263574714002501 Published online by Cambridge University Press

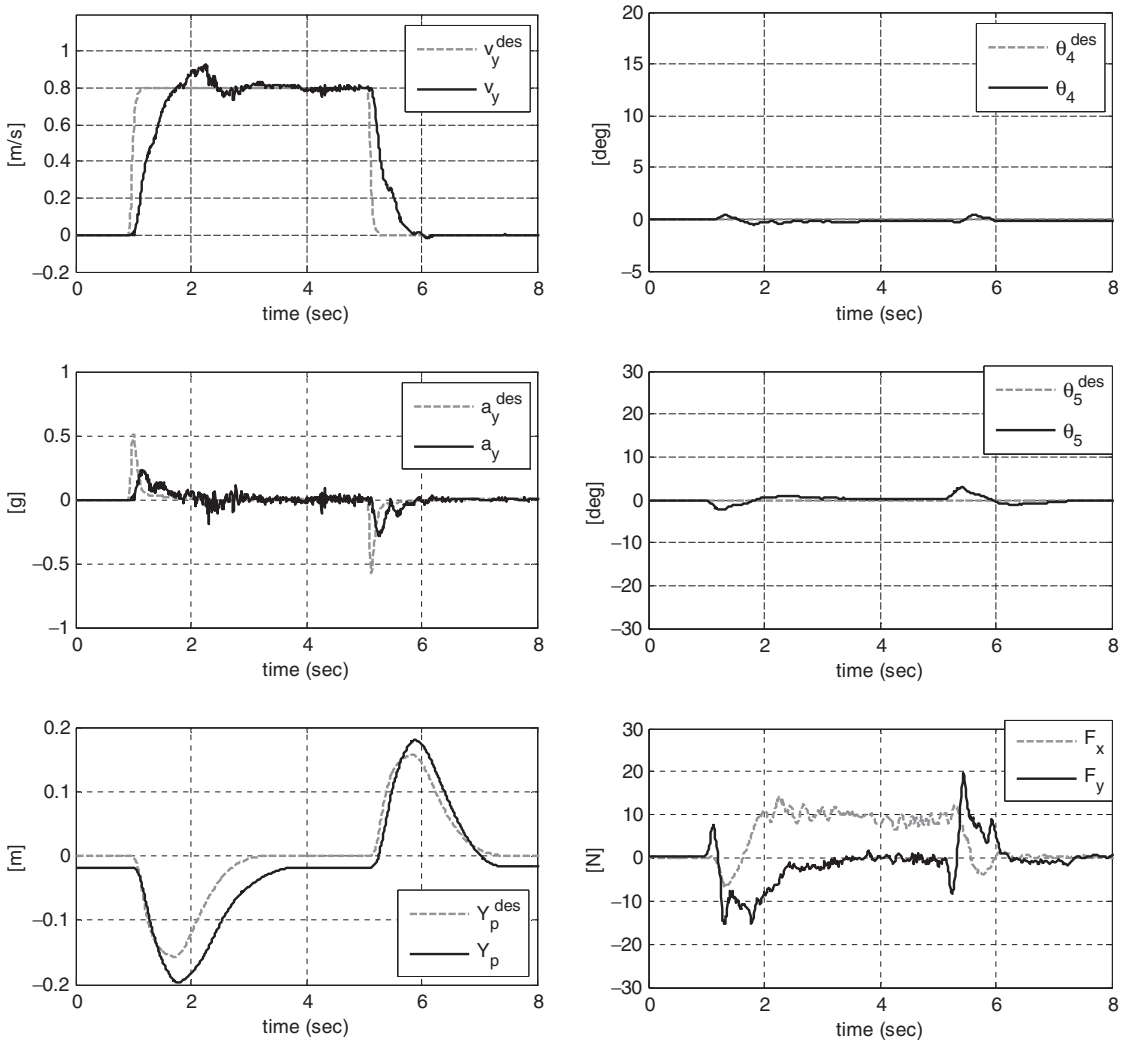

Fig. 13. Graphical results of rotational movement experiment using the SIPM.

In Fig. 12, the peak value of the *X* direction force, F_x was approximately 30 N during the deceleration period. We deduced that the ZMP becomes unstable during the deceleration period due to the tire slippage. For more stable ZMP control of the end-effector, we used the DIPM. Experiments using the DIPM are described in Section 4.2.

4.1.2. Rotational movement using SIPM. The rotational movement of the actual system was modeled as the lateral movement in the SIPM, considering offset, o_1. We used the relaxed ZMP strategy of SIPM proposed in Section 3.1 for the lateral movement. The results are shown in Fig. 13. The desired lateral velocity was given at 1 s as 0.8 m/s and the desired forward velocity was commanded as zero. The actual velocity tracked the desired value without reverse action. The manipulator tracked the desired value along the *Y* axis with tracking errors, because the gain of the Cartesian computed torque controller on the *Y* axis was chosen as a low value. This tracking error on the end-effector caused an overshoot on the velocity graph at 2 s. Nevertheless, the low gain was good for active suspension and made the end-effector more flexible. The desired orientation of the end-effector was fixed as zero. The *X* direction force, F_x in Fig. 13 was measured about 10N constantly in a rotation period. This is due to longitudinal centrifugal force. The peak force on the *Y* direction was measured at about 20 N. This is lateral centrifugal force. Both centrifugal forces cannot be compensated for in the SIPM. In the experiments of the DIPM, we will show the results of the lateral and centrifugal acceleration compensation.

https://doi.org/10.1017/S0263574714002501 Published online by Cambridge University Press

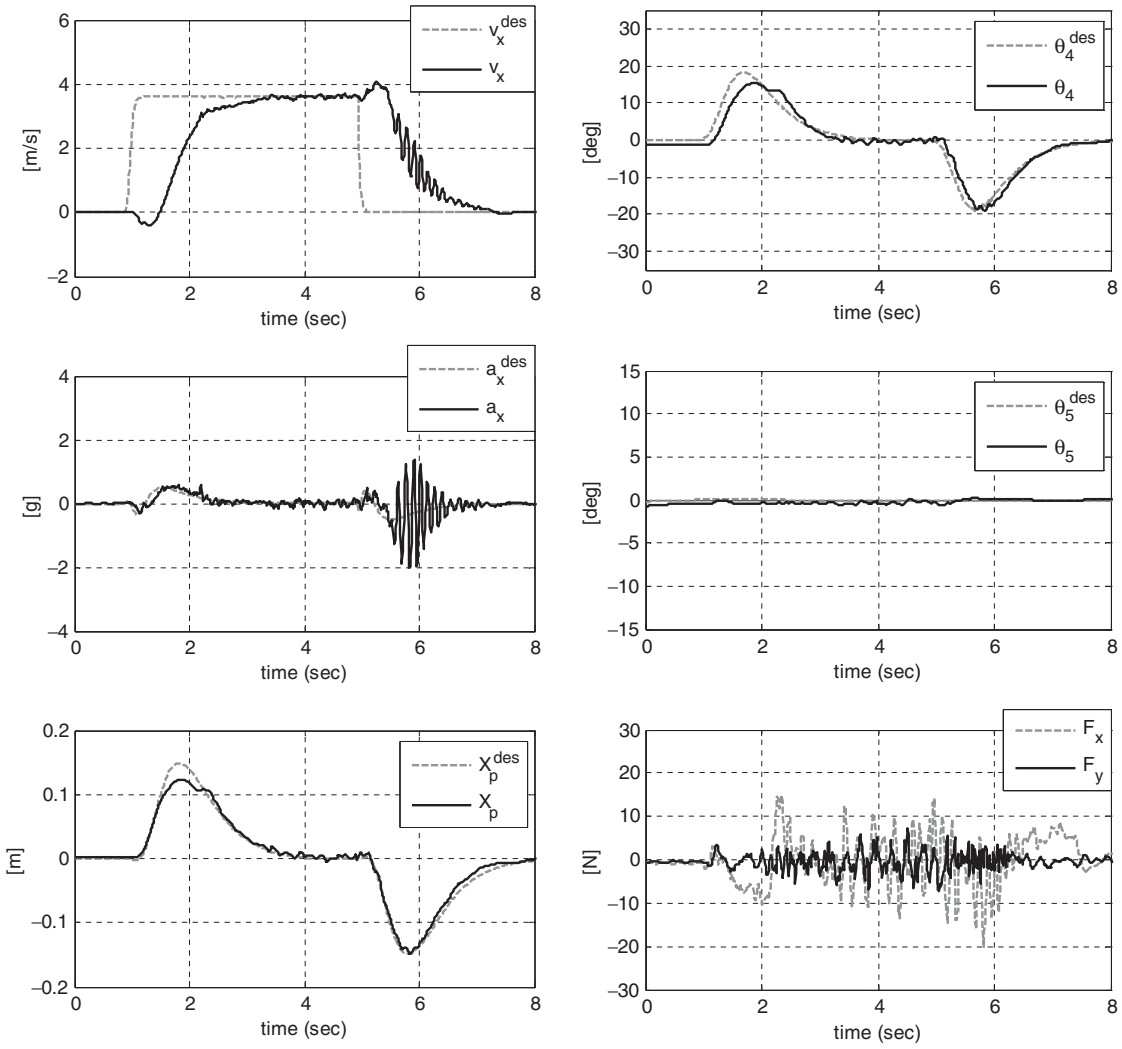

Fig. 14. Graphical results of forward movement experiment using the DIPM.

4.2. Rapid movement using DIPM

4.2.1. Forward movement using DIPM. We carried out an experiment of rapid maneuvering using KDMR-1 for the forward direction. We used the fixed ZMP strategy of DIPM proposed in Section 3.2. The manipulator was controlled by the Cartesian computed torque method using the same gain as in Section 4.1.1. For the object delivery test, we placed an object on the end-effector with no bonding. The actual behavior of the experiment is available in the webpage. (https://sites.google.com/site/dongilc27/research).

From the snapshots of the forward movement, we can see that the object was delivered safely. The graphical results of the experiment are shown in Fig. 14. The desired forward velocity was given in 1 s as 3.6m/s (13 km/hr). The actual forward velocity was controlled with a reverse action and the maximum acceleration was 0.56 g, ignoring the vibration due to tire slippage at 6 s. The X direction position of the end-effector tracked the desired value with small errors. The orientation of the end-effector was controlled according to Eq. (33). The pitch angle of the orientation θ_4 was well controlled at the desired value. The disturbance force along the X axis, F_x was quite small compared to the result using the SIPM in Fig. 12, even during the deceleration period. We concluded that the dual ZMP was stabilized by the proposed method.

4.2.2. Rotational movement using DIPM. We tested the rotational movement using the relaxed ZMP strategy of DIPM proposed in Section 3.2. The video clip of the experiment is available in the webpage. (https://sites.google.com/site/dongilc27/research).

https://doi.org/10.1017/S0263574714002501 Published online by Cambridge University Press

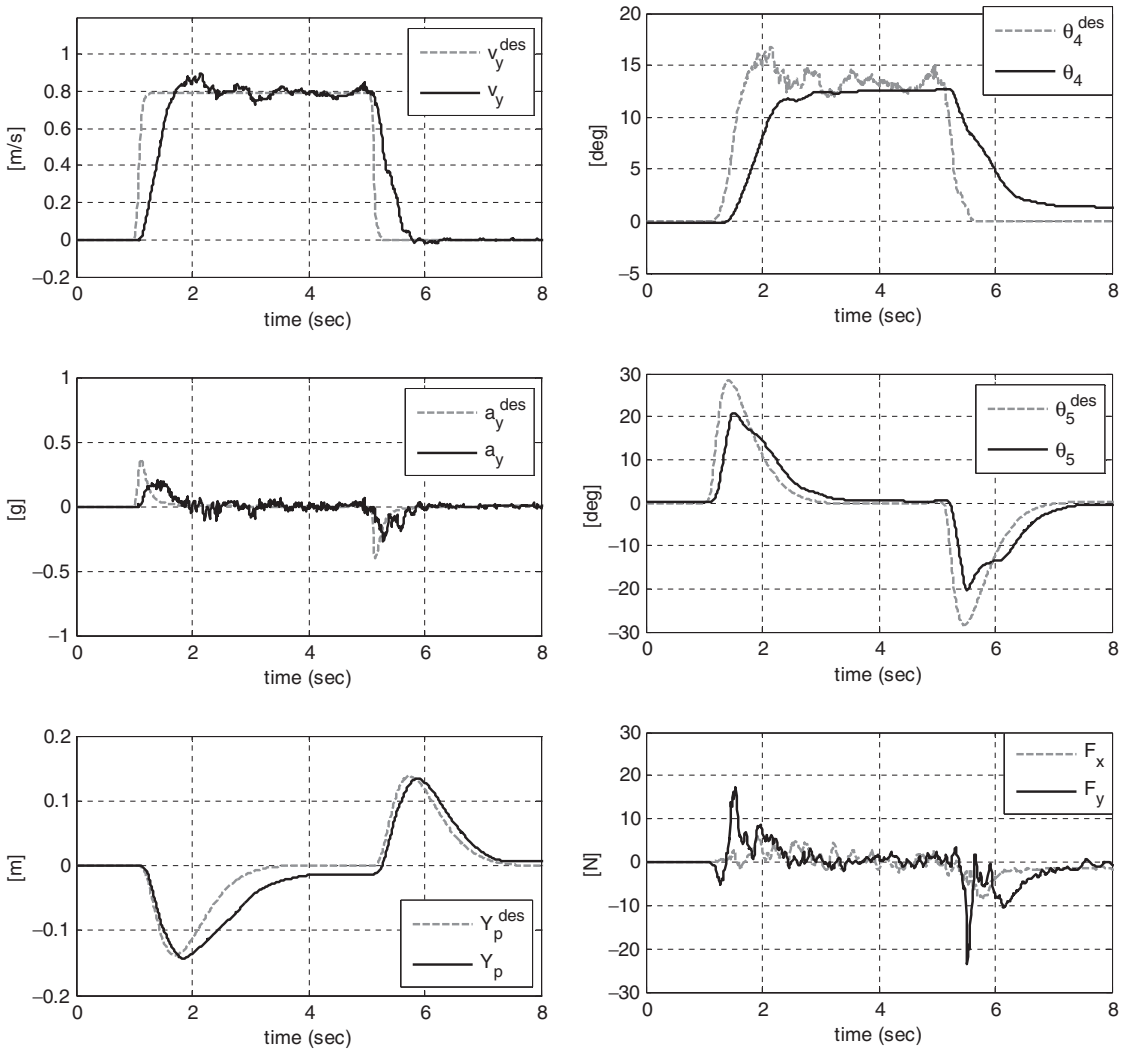

Fig. 15. Graphical results of rotational movement experiment using the DIPM.

We put the object on the end-effector and confirmed that it did not fall to the ground during the rotational movement. We designed feedback linearization to compensate centrifugal acceleration due to rotational movement. By feedback actual longitudinal velocity, v_x^{enc} and rotational velocity, $\dot{\delta}^{enc}$, we calculated desired orientation angle of the end-effector as Eq. (14). From this method, we can compensate the centrifugal acceleration therefore, only normal force is exerted on the object. It means that there is no moment on the object to make it fall. However, this is an ideal case and small moment exists in the actual experiment. By measuring moments using the FT sensor, we can observe how big moments are exerted. This method is independent on the friction coefficient and ideal for the assumption that the ground is flat. The graphical results are shown in Fig. 15. The desired lateral velocity was given at 1 s as 0.8 m/s and the desired forward velocity was set at zero. The actual velocity tracked the desired value without reverse action. The velocity tracking result of the mobile platform and the position tracking result of the manipulator were quite similar to the results of the SIPM. The desired angle of the end-effector, θ_4^{des}, θ_5^{des} was generated for the centrifugal acceleration compensation. The orientation was controlled by the PD-servo. The PD-servo gain was chosen experimentally. The position gain selected was slightly low for flexible movement. For the sake of the orientation control, disturbance forces, F_x, F_y were quite low in both X, Y directions compared. Two peaks of F_y at 1.5 s and 5.5 s were due to the limit of the angle. The range of the roll angle was limited at 30°. To track the Y axis position of the end-effector, Y_p, pendulum 1 rotated about 10°. Therefore, the roll orientation was blocked at 20°. If the possible range is enlarged, this

https://doi.org/10.1017/S0263574714002501 Published online by Cambridge University Press

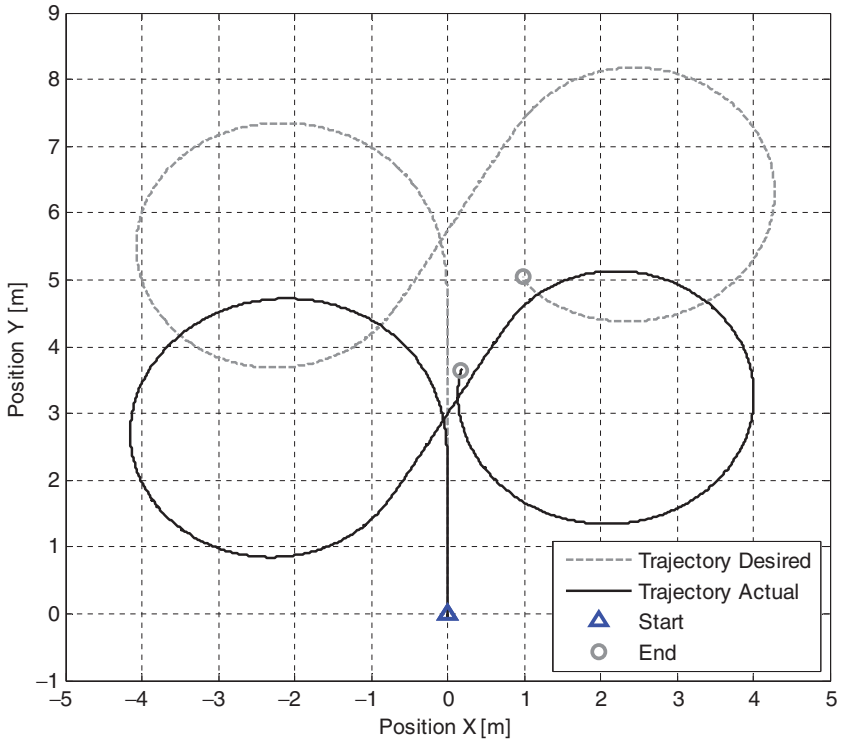

Fig. 16. (Colour online) Coupled movement trajectory of the mobile platform on the ground.

problem can be avoided. Further, if the offset, o_1, is reduced, then the centrifugal acceleration will also be reduced and the small offset will make the system more stable.

4.2.3. Coupled movement. We tested coupled movement, which occurs when the forward and rotational movements occur together. The video clip of the experiment is available in the webpage. (https://sites.google.com/site/dongilc27/research).

For forward movement, we used the fixed ZMP strategy of DIPM for higher acceleration and for rotational movement, we used the relaxed ZMP strategy of DIPM for better directional control without reverse action. Also the centrifugal acceleration was compensated by feedback linearization. The coupled movement is the toughest case to test proposed methods.

We also placed the object on the end-effector. The actual trajectory of the mobile platform was measured by encoders on the mobile platform. The resultant trajectory was in the shape of ∞, as shown in Fig. 16. On the position Y, there is quite big error between desired and actual trajectory. This is due to reverse action on the forward movement. On the other hand, the position X matches well compared to the forward movement because we used the relaxed ZMP strategy on the rotational movement. The actual trajectory had some errors due to tire slippage; however, it can be the reference of the trajectory of the mobile platform.

The graphical result of this experiment is shown in Fig. 17. We can observe reverse action on the forward velocity, v_x due to fixed ZMP strategy. The maximum forward velocity was 9.4 km/hr and the maximum rotational velocity was 100deg/s. By observing the disturbance forces, F_x, F_y in Fig. 17, we can find the disturbance forces are quite low and no offset. It means that the moment exerted on the end-effector is low, therefore we confirmed that the ZMP control and the compensation of centrifugal acceleration were performed effectively. The object delivery was also realized successfully during the coupled movement experiment. As a result, we proved the effectiveness of model-based, feed-forward ZMP control methods using DIPMs and the centrifugal acceleration compensation methods based on the feedback linearization.

https://doi.org/10.1017/S0263574714002501 Published online by Cambridge University Press

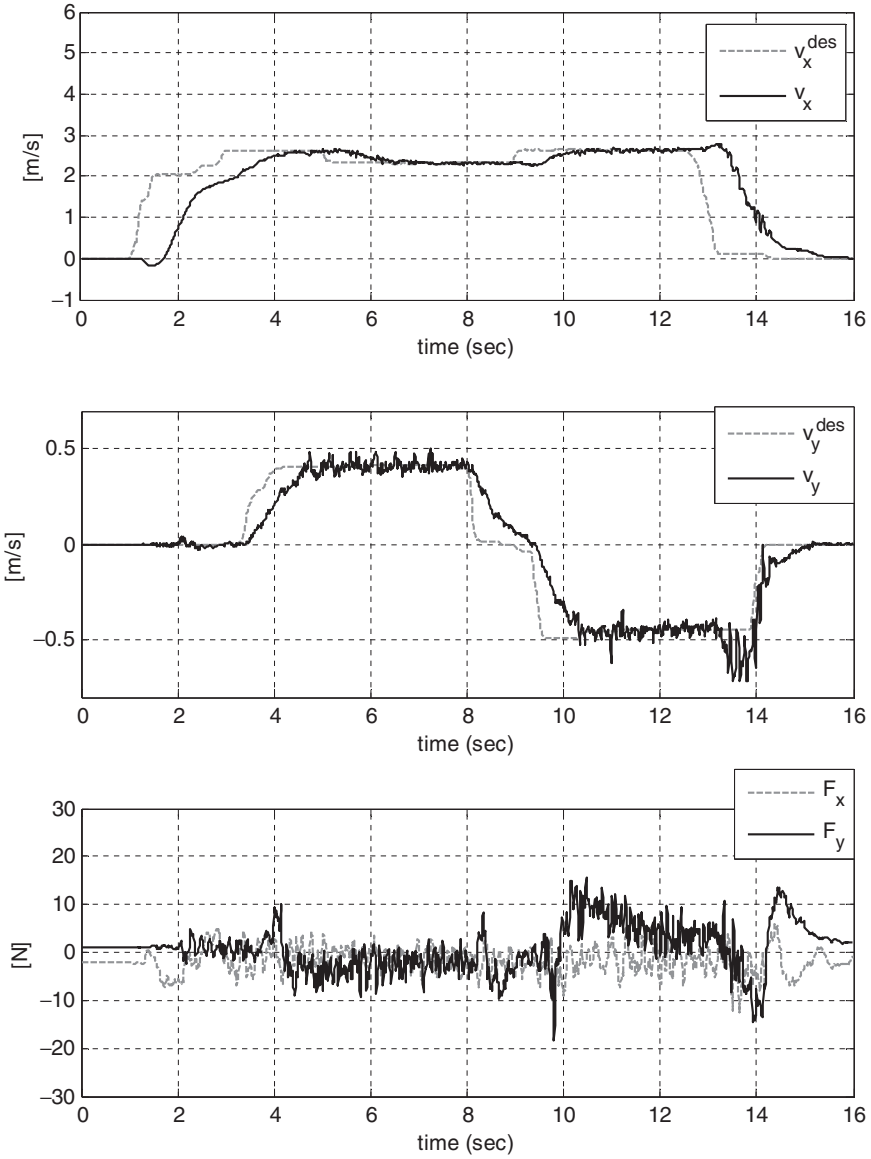

Fig. 17. Graphical results of coupled movement experiment using the DIPM.

5. Conclusions

In this paper, we have presented a novel motion planning method for an actual rapid mobile manipulator using model-based ZMP stabilization. The rapid mobile manipulator, KDMR-1, was developed for object delivery. Two kinds of linear models were introduced, SIPMs and DIPMs. In both models, we proposed a fixed and relaxed ZMP strategy using linear quadratic optimal control methods. In the SIPMs, we explored the ZMP stabilization strategies on the linearized models for rapid forward and rotational movements. In the DIPMs, we considered centrifugal acceleration in coupled movement. To compensate for centrifugal accelerations, we decoupled the system as two linearized models based on the feedback linearization method. In the decoupled models, we applied the ZMP stabilization strategies for rapid object delivery.

The experimental results using SIPMs showed that the maximum acceleration was approximately 0.8 g and the maximum velocity was 13 km/hr. The experimental results using the DIPMs showed that it is possible to deliver an object safely in forward, rotational and coupled movements with high acceleration and speed (maximum 0.56 g, 13 km/hr). Experimental results showed the effectiveness of the proposed methods and the high mobility of KDMR-1.

https://doi.org/10.1017/S0263574714002501 Published online by Cambridge University Press

In the experiment of rotational movement using DIPM, the roll orientation reached the limit angle. For higher acceleration performance, we found that it was necessary either to enlarge the range of the joint angle or reduce the offset, o_1. By redesigning a whole new rapid mobile manipulator, we will achieve a wider range of the joint angle and better acceleration performance. We will implement a laser finder and a stereo vision sensor in the new rapid mobile manipulator. The sensors will be used for localization and stabilization purposes. The reverse action in the fixed ZMP strategy was inevitable due to the non-minimum phase characteristic. In the relaxed ZMP strategy, there is no reverse action. However, the acceleration performance depended greatly on the size of the supporting polygon. If we know the location of obstacles in advance, we can select the better strategy between the fixed ZMP and relaxed ZMP. For a sudden obstacle, we need the fixed ZMP strategy and for a moderate obstacle, the relaxed ZMP strategy is sufficient. The switching algorithm of ZMP strategies will be studied with the new rapid mobile manipulator and reported by our group.

References

1. S. Dubowsky and E. E. Vance, "Planning Mobile Manipulator Motions Considering Vehicle Dynamic Stability Constraints," *Proceedings of the IEEE International Conference on Robotics and Automation*, Scottsdale, AZ, USA, (1989) pp. 1271–1276.
2. T. Fukuda and Y. Fujisawa, "Manipulator/Vehicle System for Man-Robot Cooperation," *Proceedings of the IEEE International Conference on Robotics and Automation*, Nice, France, (1992) pp. 74–79.
3. Q. Huang, K. Tanie and S. Sugano, "Coordinated motion planning for a mobile manipulator considering stability and manipulation," *Int. J. Robot. Res.* **19**(8), 732–742 (2000).
4. J. Kim and W. K. Chung, "Real-time zero moment point compensation method using null motion for mobile manipulators," *Adv. Robot.* **20**(5), 581–593 (2006).
5. E. Papadopoulos and D. A. Rey, "The force-angle measure of tipover stability margin for mobile manipulators," *Veh. Syst. Dyn.* **33**(1), 29–48 (2000).
6. S. A. A. Moosavian and K. Alipour, "Tip-Over Stability of Suspended Wheeled Mobile Robots," *Proceedings of the IEEE International Conference on Mechatronics and Automation*, Harbin, P.R. China, (2007) pp. 1356–1361.
7. S. Lee, M. Leibold, M. Buss and F. C. Park, "Online Stability Compensation of Mobile Manipulators Using Recursive Calculation of ZMP Gradients," *Proceedings of the IEEE International Conference on Robotics and Automation*, Saint Paul, Minnesota, USA, (2012) pp. 850–855.
8. J. Kim, W. K. Chung, Y. Youm and B. H. Lee, "Real-time ZMP Compensation Method using Null Motion for Mobile Manipulators," *Proceedings of the IEEE International Conference on Robotics and Automation*, Washington, DC, USA, (2002) pp. 1967–1972.
9. M. Kim, D. Choi and J.-H. Oh, "Stabilization of a Rapid Four-wheeled Mobile Platform Using the ZMP Stabilization Method," *Proceedings of the IEEE/ASME International Conference on Advanced Intelligent Mechatronics*, Montreal, Canada, (2010) pp. 317–322.
10. D. Choi, M. Kim and J. H. Oh, "Development of a rapid mobile robot with a multi-degree-of-freedom inverted pendulum using the model-based zero-moment point stabilization method," *Adv. Robot.* **26**(5–6), 515–535 (2012).
11. D. Choi and J. Oh, "ZMP Stabilization of Rapid Mobile Manipulator," *Proceedings of the IEEE International Conference on Robotics and Automation*, St. paul, USA, (2012) pp. 883–888.
12. S. Kajita, F. Kanehiro, K. Kaneko, K. Fujiwara, K. Harada, K. Yokoi and H. Hirukawa, "Biped Walking Pattern Generation by using Preview Control of Zero-Moment Point," *Proceedings of the IEEE International Conference on Robotics and Automation*, Taipei, Taiwan, (2003) pp. 1620–1626.
13. T. Sugihara, Y. h. Nakamura and H. Inoue, "Realtime Humanoid Motion Generat ion through ZMP Manipulation based on Inverted Pendulum Control," *Proceedings of the IEEE International Conference on Robotics and Automation*, Washington, DC, USA, (2002) pp. 1404–1409.
14. I.-W. Park, J.-Y. Kim and J.-H. Oh, "Online walking pattern generation and its application to a biped humanoid robot — KHR-3 (HUBO)," *Adv. Robot.* **22**(2), 159–190 (2008).
15. D. Choi, "Development of a Rapid Mobile Manipulator and Model-based Stabilization Methods," *Proceedings of the Mechanical Engineering*, KAIST, Daejeon, (2012).
16. M. Vukobratovic and B. Borovac, "Zero-moment point — thirty five years of its life," *Int. J. Humanoid Robot.* **1**(1), 157–173 (2004).
17. S. Sugano, Q. Huang and I. Kato, "Stability Criteria in Controlling Mobile Robotics Systems," *Proceedings of the IEEE International Conference on Intelligent Robots and Systems*, Tokyo, Japan, (1993) pp. 832–838.
18. Napoleon, S. Nakaura and M. Sampei, "Balance Control Analysis of Humanoid Robot based on ZMP Feedback Control," *Proceedings of the IEEE International Conference on Intelligent Robots and Systems*, EPFL. Lausanne, Switzerland, (2002) pp. 2437–2442.
19. D. Choi and J.-h. Oh, "Development of cartesian arm exoskeleton system (CAES) using 3-axis force/torque sensor," *Int. J. Control, Autom. Syst.* **11**(5), 976–983 (2013).
20. D. Choi and J.-H. Oh, "Four and Two Wheel Transformable Dynamic Mobile Platform," *Proceedings of the IEEE International Conference on Robotics and Automation*, Shanghai, P.R. China, (2011) pp. 1–4.

https://doi.org/10.1017/S0263574714002501 Published online by Cambridge University Press

21. D. Choi and J.-H. Oh, "Human-Friendly Motion Control of a Wheeled Inverted Pendulum by Reduced-Order Disturbance Observer," *Proceedings of the IEEE International Conference on Robotics and Automation*, Pasadena, USA, (2008) pp. 2521–2526.
22. D. Choi and J.-H. Oh, "Active Suspension for a Rapid Mobile Robot Using Cartesian Computed Torque Control," in *Journal of Intelligent and Robotic Systems*, published in Online First, (2014).

Appendix

A1. Development of a rapid mobile manipulator: KDMR-1.
We developed a rapid mobile manipulator with 5-DOF (Degrees of Freedom) called KDMR-1 (KAIST Dynamic Mobile Robot-1). The configuration of the rapid mobile manipulator is shown in Fig. 18. The specifications of KDMR-1 are summerized in Table III, IV. Our target mobile robot consists of two parts: a mobile platform and a 5-DOF manipulator. The mobile platform consists of two active rear wheels and two front caster wheels. A 3-axis force/torque (FT) sensor developed in the previous research[19] is mounted on the end-effector to measure the external disturbance forces. There is 6 kg of mass above the force-torque sensor. The space between the mobile platform and the end-effector is composed of a 5-DOF manipulator that moves the mass. The kinematic relationship of the 5-DOF manipulator is shown in Fig. 19.

The 5-DOF manipulator moves along the X, Y, Z direction, and the end-effector rotates about the X, Y axis in Cartesian coordinates. The position of the end-effector is determined by $\theta_1, \theta_2, \theta_3$. The orientation of the end-effector is determined by θ_4, θ_5. The main purpose of the KDMR-1 is rapid object delivery in open spaces like conference halls, shopping malls, hospitals, and so on. If we put objects on the end-effector, we need an effective vibration damping control algorithm for high speed delivery. By using the 5-DOF manipulator, we suppressed the vibrations along the X, Y, Z direction. The rapid mobile platform is designed to transform from a four-wheel drive mode to a two-wheel drive mode. The transformation is accomplished by the conversion algorithm.[20] There are two kinds of modes in the two wheel drive mode, the self-balancing mode and the human-riding mode. In the self-balancing mode, we controlled the two-wheeled inverted pendulum with a balancing algorithm. In the human-riding mode, a person can ride on the human riding support and control the mobile platform using the 5-DOF manipulator.

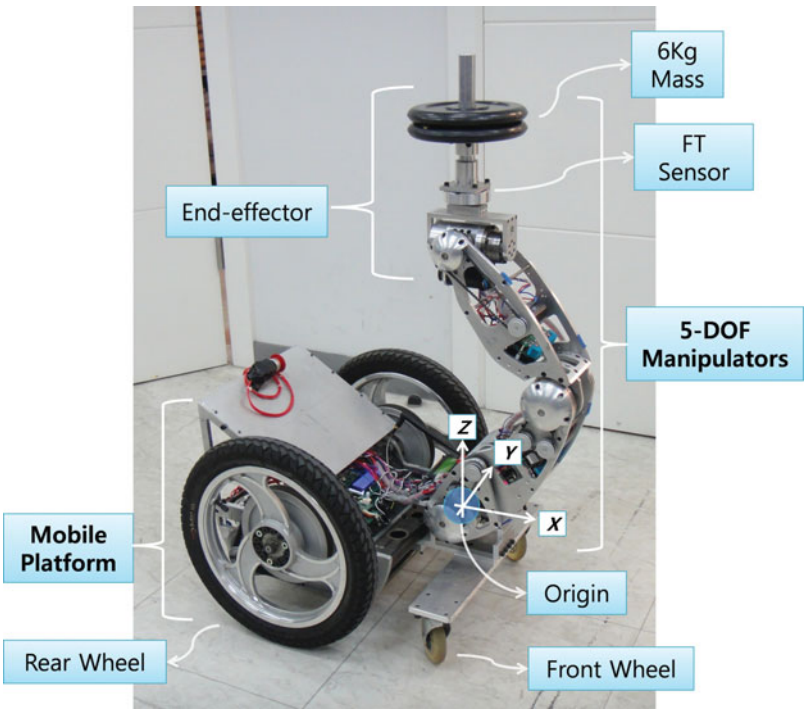

Fig. 18. (Colour online) KAIST Dynamic Mobile Robot (KDMR-1).

https://doi.org/10.1017/S0263574714002501 Published online by Cambridge University Press

Table III. Specifications of the mobile platform of KDMR-1.

DOF	2
Platform size	540 mm × 540 mm × 400 mm
Wheel size	16 inch (rear wheels), 4 inch (front wheels)
Weight	39.1 kg
Payload	Up to 100 kg (including human-riding condition)
Maximum speed	12 km/hr (speed limited for safety) 32 km/hr (maximum possible speed)
Maximum acceleration	0.6 g
Actuator	1 kW high power DC motor with 2-stage pulley & belt system (13.7:1)
Motor control unit	2-ch high power motor controller
Sensory devices	Encoder, 2EA, IMU for pitch direction, 1EA (tilt sensor & Gyro sensor fusion)
Power supply	24 V – 7Ah LEAD acid battery, 2EA (parallel connection, total 14Ah)
Operating device	TMS320F2808, 1EA
Communication	CAN, SCI, bluetooth v2.0 + EDR class 1
Controllable distance	Up to 400 m

Table IV. Specifications of the manipulator of KDMR-1..

DOF	5	
Link length	0.3 m (θ_1&$\theta_2 \rightarrow \theta_3$), 0.3 m ($\theta_3 \rightarrow \theta_4$&$\theta_5$)	
Work volume	Translation	X direction: ± 270 mm Y direction: ± 160 mm Z direction: 350 600 mm
	Rotation	X axis: ± 30° Y axis: ± 120°
Weight	19.8 (include 6 kg mass)	
Payload	Up to 9 kg (dynamic load), up to 20 kg (static load)	
Actuator	200W DC servo motor with harmonic gear, pulley & belt, planetary gear	
Motor control unit	2-ch joint motor controller	
Sensory devices	Encoder, 5EA, 3-axis force-torque sensor, 1EA	
Power supply	24V, 12V	
Operating device	Embedded PC with wireless LAN	
Communication	CAN	

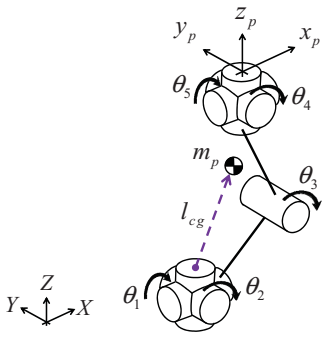

Fig. 19. (Colour online) 5-DOF Manipulator.

The Huboway platform developed by Choi[21] was tuned for a rapid mobile manipulator. The original Huboway platform was developed as a human transporter that balances itself on two wheels using an IMU (Inertia Measurement Unit) sensor and a balancing algorithm. In our research, we attached two caster wheels onto the Huboway platform. The tuned mobile platform is capable of 12 km/hr, the maximum safe speed at which it can operate.

https://doi.org/10.1017/S0263574714002501 Published online by Cambridge University Press